Version of Record: https://www.sciencedirect.com/science/article/pii/S0022309321002957
Manuscript_11df3f1d824109ca1917d96163735e3e

Investigation of alumino-silicate glasses by coupling experiments and simulations: Part I - Structures

J.-M. Delaye[1*], A. Le Gac[1], S. Macaluso[1], F. Angeli[1], F. Lodesani[2], T. Charpentier[2], S. Peuget[1]

[1]CEA, DES, ISEC, DE2D, University of Montpellier, Marcoule, F-30207 Bagnols-sur-Cèze, France
[2]Université Paris-Saclay, CEA, CNRS, NIMBE, 91191 Gif-sur-Yvette Cedex, France

Abstract

A set of alumino-silicate glasses with SiO_2-Al_2O_3-Na_2O-CaO compositions was investigated using Raman and NMR spectroscopy techniques and by classical molecular dynamics, in order to study the structural modifications which occur when CaO progressively replaces Na_2O and when Al_2O_3 progressively replaces SiO_2. The effect of a gradual increase in the Al_2O_3 content was also studied. Al was always 4 coordinated for all the compositions studied, including the peraluminous glasses. An increase in the number of Al-O-Al bonds was found when the Al_2O_3 or CaO content increases. The study confirmed that AlO_4 groupings are preferentially compensated by Na rather than by Ca, and that there are non-bridging oxygens surrounded by mixed environments containing both Na and Ca. Combining the information given by the Raman and NMR spectroscopy results enabled the attribution of the Raman band at 570cm^{-1} to the Si-O-Al bonds. It confirmed that the band at 510cm^{-1} can be attributed to the Al-O-Al bonds, while that at 985cm^{-1} can be attributed to the Q4-Al entities. Lastly, it was demonstrated that the classical molecular dynamics potentials of Deng et al., specifically developed for this type of glasses, permit the reproduction of a large number of the experimental results quantitatively or sometimes simply qualitatively.

Keywords: Alumino-silicate glasses, structure, Raman, NMR, Molecular dynamics

1. Introduction

Alumino-silicate glasses have been widely studied, as they are very important materials from the geological point of view. Their special features, including hardness and optical properties, also interest different industries (optic fibers, electronic devices …). In the nuclear industry, this type of matrix is also considered for the containment of high level radioactive waste [1,2].

A certain amount of information is already available in the literature concerning the SiO_2-Al_2O_3-Na_2O-CaO compositions studied here [3,4,5,6]. The elements Si and Al, network formers, organize themselves in a cross-linked network of SiO_4 and AlO_4 tetrahedrons. The negative charge of the AlO_4 groups is compensated by the modifying elements Na and Ca. It has been seen that the charge compensation takes place from the Na in priority when the elements Na and Ca are both present, with the Ca forming non-bridging oxygens around the Si [7,8,9,10,11].

* Corresponding author

It should be noted that in glasses for which all the Al cannot be compensated by modifiers (peraluminous glasses, characterized by a ratio ($[Na_2O]+[CaO])/[Al_2O_3] < 1$), certain studies have concluded on the presence of 5 or 6-coordinated Al. Some even evoke the possibility of finding 5 or 6-coordinated Al in peralkaline glasses (glasses characterized by a ratio $[Na_2O]+[CaO])/[Al_2O_3] > 1$). To date, there has been no consensus on this question [12,13,14,15,16].

At the medium range order, the Loewenstein's exclusion rule [17] first proposed for crystals and then extended to alumino-silicate glasses, has in general been verified. This rule states that Al atoms exclude each other, i.e. that it is not possible to form Al-O-Al bonds. But the rule seems less certain, especially in situations when the CaO concentration becomes higher. In this case, the presence of Ca enables the formation of Al-O-Al bonds [16,18,19,20].

The angular distributions within the cross-linked network formed by the Si and the Al evolve with the quantities of SiO_2 and Al_2O_3. In particular, a decrease in the Si-O-Si angle has been observed when the $[Al]/([Al]+[Si])$ ratio increases.

Concerning the distribution of the alkali and alkaline earth elements, it has been shown that these can concentrate in certain zones and form percolation channels, which then impact the properties of the material and particularly its dynamic properties [21,22,23,24].

Many studies have been carried out on alumino-silicate glasses using molecular modeling [6,25,26,27,28,29,30,31] and today several potentials are proposed to simulate such compositions. Recent work by Lodesani et al. [24] compared different available potentials with each other in silicate glasses containing both Na_2O and K_2O. It seems that the Shell Model type potentials [32] give overall better performances in reproducing both the structure and the diffusive mechanisms in this type of glass. In the study described here, this type of potentials was not used as our final objective was to correlate ballistic damage with the chemical compositions of alumino-silicate glasses. It is known that calculations with Shell Model type potentials present mathematical instabilities during simulation of displacement cascades because of the very strong strains imposed on the ionic local environments. This was the reason for using rigid ions in this study.

The work presented here concerns the structure of a set of peralkaline and peraluminous $SiO_2 – Al_2O_3 – Na_2O – CaO$ glasses. Three series of glasses were defined to identify the impact of exchanging CaO for Na_2O, of exchanging Al_2O_3 for SiO_2, and finally the impact of an increasing Al_2O_3 content. In the second paper associated to this one, the behavior of these glasses under irradiation will be presented.

The originality of this approach is that it couples three complementary techniques to characterize a large range of $SiO_2 – Al_2O_3 – Na_2O – CaO$ glass compositions. These techniques were Raman spectroscopy, suitable for investigating the structural medium range order structure, solid state high-resolution magic angle spinning nuclear magnetic resonance (MAS NMR) spectroscopy, well adapted to characterize local environments, and classical molecular dynamics, which accesses both the local order and the medium range order, but for which precision can be limited depending on the quality of the force field used.

2. Methods

2.1 Glass fabrication

The 13 vitreous compositions selected for the experiments are distributed in three series, and are listed in Table 1.
In series 1, only the Na_2O/CaO ratio varies (the oxide CaO progressively replaces the oxide Na_2O) but the theoretical percentage of NBOs (NBO = Non Bridging Oxygen) remains more or less constant.

For a given composition, the molar percentage of NBOs is calculated as follows:

$$\%NBO = 100 * \frac{2*([Na_2O]+[CaO]-[Al_2O_3])}{2*[SiO_2]+[Na_2O]+[CaO]+3*[Al_2O_3]} \quad (1)$$

It is simply the quantity of charges which form NBO, i.e. the quantity of Na and Ca charges which do not compensate the Al, divided by the total quantity of O.

In series 2, the oxide Al_2O_3 progressively replaces the oxide SiO_2 and the Na_2O/CaO ratio remains constant. The theoretical percentage of NBOs also remains more or less constant.
In series 3, the oxide Al_2O_3 increases progressively and the other oxides are normalized to keep the molar ratios constant. The percentage of NBOs diminishes progressively. This series contains both peralkaline and peraluminous glasses.

The glasses were prepared in two steps, the first corresponding to the precursor fusion (CaO, Na_2CO_3, Al_2O_3, SiO_2) followed by quenching, and the second to re-fusion followed by annealing. These two steps enabled homogenous glasses to be obtained and the release of internal stresses.

The initial powders were heated slowly in order to decompose the carbonates, and then melted for 3 hours in a platinum-rhodium crucible (Pt-Rh) at a temperature between 1350°C and 1450°C depending on the chemical compositions. The melted glass was quenched in air on a steel plate, and then the glass was ground and re-melted at 1350°C in a platinum-gold crucible (Pt-Au) in order to simplify de-molding at the end of the cycle. After 30 minutes, the melted glass was quenched from 1350°C to 600°C in air. The glass was then maintained at 600°C for 1 hour. Then a slow quench to ambient temperature (0.5°C/min) is applied.

Some alumino-silicate glasses rich in aluminum and in calcium showed a strong tendency to de-vitrify (the Ca, Si/Al 2.4, Si/Al 1.6, Si/Al 1.4 and Si/Al 1.3 glasses). These were therefore synthetized by heating the precursors slowly to decompose the carbonates, and then melting them in a zirconia crucible (ZrO_2) at a temperature between 1500°C and 1600°C for 3 hours. They were quenched by pouring the melted glass into a graphite carbon mold. The glasses were next annealed at 600°C for 1 hour. Then a slow quench to ambient temperature (1°C/min) is applied.

The compositions given in Table 1 were measured by EDS after glass fabrication.

Series 1	**SiO_2**	**Na_2O**	**Al_2O_3**	**CaO**
Na	65.6	27.1	7.4	0.0
Na/Ca 1.4	59.9	19.8	6.6	13.7
Na/Ca 0.3	58.0	9.1	6.5	26.4
Ca	55.6	0.0	7.3	35.5

Series 2	SiO_2	Na_2O	Al_2O_3	CaO
NBO1	66.0	19.1	2.8	12.1
NBO2	62.6	19.5	5.4	12.5
Na/Ca 1.4	59.9	19.8	6.6	13.7
NBO4	57.0	20.4	8.0	14.6
NBO5	52.1	22.0	10.6	15.3

Series 3	SiO_2	Na_2O	Al_2O_3	CaO
Na/Ca 1.4	59.9	19.8	6.6	13.7
Si/Al 5.4	55.6	20.3	10.3	13.9
Si/Al 2.4	48.7	18.0	20.7	12.6
Si/Al 1.6	43.9	16.5	28.3	11.3
Si/Al 1.4	41.7	14.4	29.8	13.8
Si/Al 1.3	41.4	15.3	31.8	11.3

Table 1: Series of glasses selected for the experiments. The compositions in molar percentages were measured by EDS.

2.2 Spectroscopic methods: Raman and MAS NMR

The glasses were analyzed by Raman spectroscopy. The Raman spectrometer used was an X-ploRA+ (Horiba). The acquisitions were carried out with a 532nm laser between 55cm^{-1} and 1700cm^{-1}. The axial (in depth) and lateral resolutions were respectively 3µm and 0.7µm, and the spectral resolution was 1.7cm^{-1}.
Each spectrum shown in this article corresponds to an average of 10 spectra acquired during 20s at different places on the glass surface. The raw spectra were corrected for temperature and for frequency with Long's correction [33] and normalized to the total area between 55cm^{-1} and 1300 cm^{-1}.

The glasses were also characterized by MAS NMR of sodium-23, aluminum-27 and silicon-29. Some glass compositions were labelled in oxygen-17 for ^{17}O MAS NMR data. The data were collected on a Bruker Avance II 500WB spectrometer (operating at a magnetic field of 11.72T) using a commercial CPMAS Bruker 4mm probe (outer-diameter of rotor made of ZrO_2) at a spinning frequency of 12.5 kHz. The ^{27}Al and ^{23}Na spectra were acquired using a single short-pulse RF (1µs), enabling homogenous excitation of all the environments (quantitative spectrum), and a repetition time of 0.5s. Two-dimensional ^{23}Na and ^{27}Al MQMAS spectra were collected on representative compositions using the Z-filter pulse sequence [34,35]. A 1M $AlCl_3$ solution was used as external reference for ^{27}Al NMR spectra (0 ppm) and ^{23}Na chemical shifts was referenced to a 1M NaCl solution (0 ppm). For ^{29}Si, a Carr–Purcell–Meiboom–Gill (CPMG) pulse sequence [36] was used with a recycle delay of 20s (no change in lineshape was observed for longer recycle delay of 200s). The spectra are referenced to an external tetrakistrimethylsilane (TKS) sample for which the highest intensity peak is situated at -9.9 ppm from that of tetramethylsilane (TMS).
^{17}O MAS spectra were acquired with a rotor-synchronized spin echo sequence (echo delay of one rotor period) with selective pulses on the central transition. This pulse sequence enabled a quantitative spectrum to be acquired (repetition delay of 1s) without base line distortions. ^{17}O MQMAS NMR were collected on Bruker Avance Neo 300SWB spectrometer (operating at a magnetic field of 7.05T) at a spinning frequency of 12.5 kHz with a CPMAS Bruker 4mm probe. A shifted-Echo pulse sequence was used [35] with an echo delay of 2ms. Spectra are

referenced to an external sample of liquid $H2^{17}O$ (0 ppm). A lower field was chosen to perform such experiments as we observed a better resolution (vs 11.75T) in the MQMAS spectra. Such a comparison if out of the scope of the present work and will be presented elsewhere.

2.3 Glass simulation

Seven glasses were simulated (the Na, Na/Ca 1.4, Na/Ca 0.3, Ca, Si/Al 5.4, Si/Al 2.4, and Si/Al 1.3 glasses) by classical molecular dynamics with the DLPOLY code [37].
First, a liquid was equilibrated at 4000K for 100ps in the NVT ensemble (constant Number of atoms, Volume and Temperature), then a 10^{12} K/s quench is applied to obtain a solid structure at 300K. The quenching was carried out by maintaining the volume constant and by reducing the temperature by 100K steps. Finally, a relaxation at 300K was applied in the NVE ensemble (constant Number of atoms, Volume and Energy) for 5ps.

For each step in the glass simulations, the time step was equal to1fs.
The cubic simulation boxes contained 60000 atoms. The volume (which remained constant throughout the preparation) was adjusted so as to reproduce the experimental density.

The force fields applied were the Buckingham potentials fitted by Deng et al. for this type of composition [38,39]:

$$V_{ij}(r_{ij)} = \frac{z_i z_j}{r_{ij}} + A_{ij}\exp(-\frac{r_{ij}}{\rho_{ij}}) - \frac{C_{ij}}{r_{ij}^6} \qquad (2)$$

$V_{ij}(r_{ij})$ corresponds to the energy attributed to a pair of atoms i and j separated by a distance r_{ij}. The first term corresponds to the Coulomb interaction (z_i and z_j are the charges of the atoms). The second term corresponds to a steric repulsion, and the last to a dipolar interaction. A_{ij}, ρ_{ij} and C_{ij} are adjustable parameters. The values for the adjustable parameters are available in the reference [38].

3. Results

3.1 Raman spectroscopy

3.1.1 Presentation of the overall spectra

The Raman spectra for the three series of glasses are shown in Figure 1.

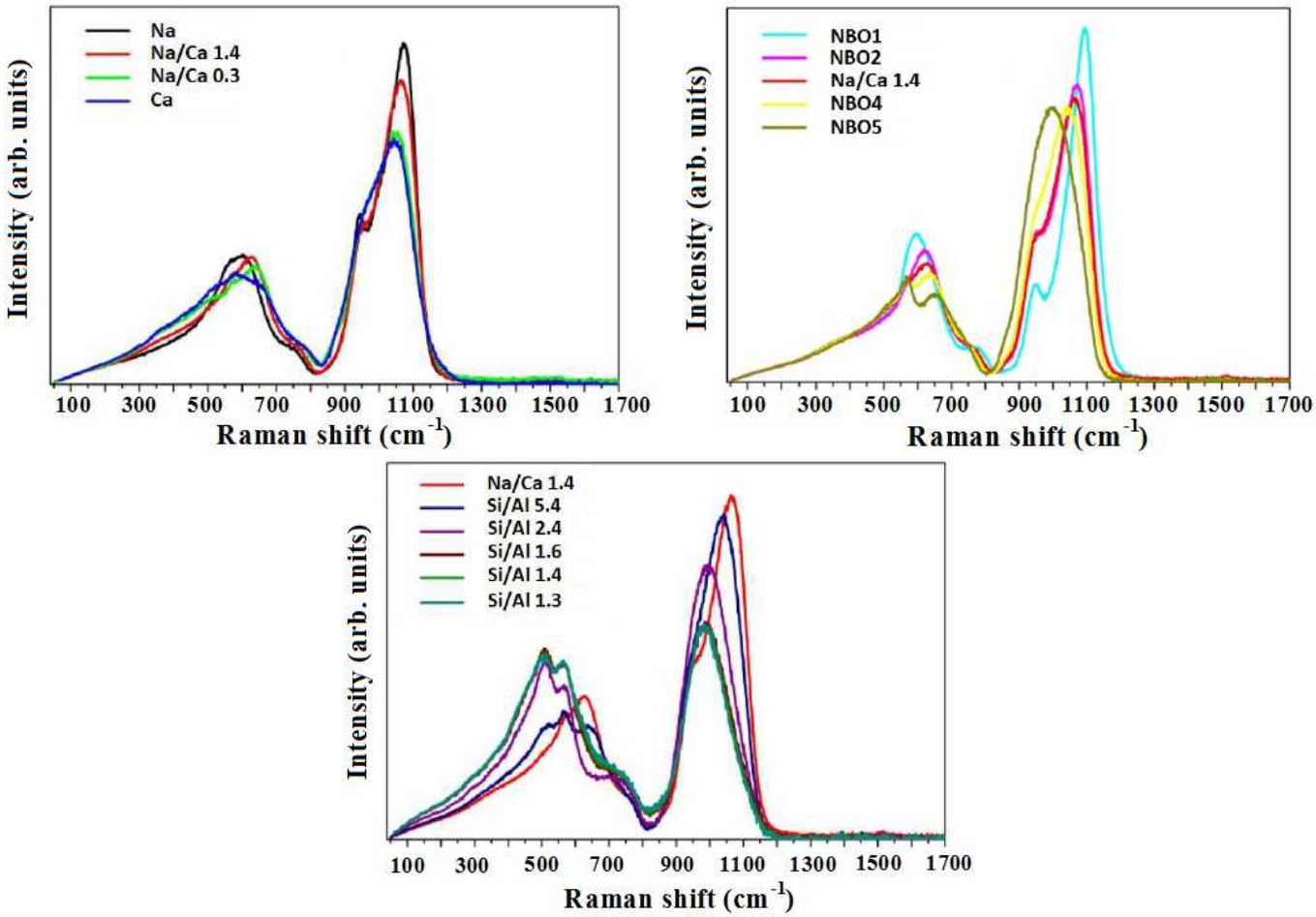

Figure 1: Raman spectra for the three series of glasses. The intensities have been normalized for the spectrum areas.

Two regions in the spectra are separated, between 450cm^{-1} and 825cm^{-1}, and between 825cm^{-1} and 1300cm^{-1}, and each of these regions will be discussed separately.

3.1.2 Region between 450cm^{-1} and 825cm^{-1}

Zooms taken on the spectra in the region between 450cm^{-1} and 825cm^{-1} for the three series of glasses are shown in Figure 2.

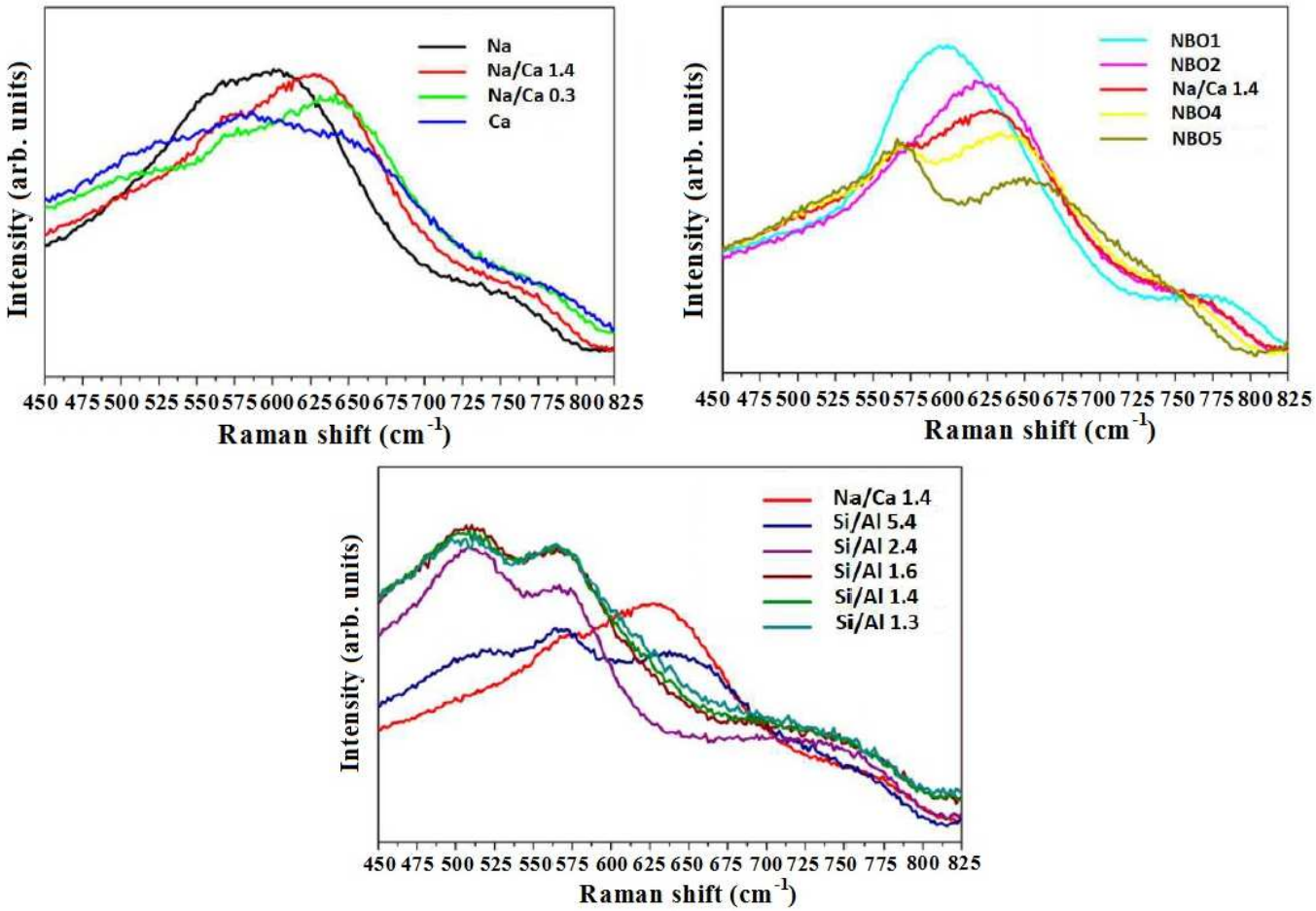

Figure 2: Raman spectra for the three series of glasses. Zoom between 450 cm^{-1} and 825 cm^{-1}

The main contributions are located at 510cm^{-1}, 570cm^{-1} and 600cm^{-1}. The origin of these bands has been attributed to the vibrations of the T-O-T bonds (T=Si or Al) [40,41].
The first point to note is the evolution of the shape of the spectra in series 2 at around 600cm^{-1}. A clearly visible peak for the NBO1 glass progressively loses intensity and shifts towards higher frequencies when the Al_2O_3 content increases to the detriment of the SiO_2 content.
This can be interpreted as a decrease in the Si-O-Si angle as the local environment of the Si atoms contains increasing numbers of Al.
This observation also holds when the spectra of the series 3 Na/Ca1.4 and Si/Al5.4 glasses are compared. The peak is no longer visible for the glasses with the highest Al_2O_3 contents.

A similar shift appeared for the series 1 glasses when CaO progressively replaced Na_2O. Here, the origin of the shift is different, because the Si/Al ratio is constant in the series 1 glasses.
The replacement of Na ions by Ca ions in the vicinity of Si ions thus also leads to the closing of Si-O-Si angles. Such a process had already been proposed in the literature [42,43].

The gradual replacement of SiO_2 by Al_2O_3 in the series 2 glasses means the emergence of a contribution at 570cm^{-1} and a shoulder at 510cm^{-1}. These contributions are generally associated with the Si-O-Al and Al-O-Al bonds, although their precise frequency positions continue to be debated [5,40]. Nevertheless, it seems that in the case of the glasses investigated here the increase in the Al_2O_3 content to the detriment of SiO_2 leads to the formation of a significant quantity of Al-O-Al bonds. The existence of Al-O-Al bonds in alumino-silicate glasses has already been proposed in the literature on the basis of

spectroscopic studies or of molecular simulations [18,20], even though this contradicts the Loewenstein's exclusion rule. The rise of the bands at 570cm^{-1} and 510cm^{-1} with the increased Al_2O_3 content of the series 3 glasses confirms the proposed attribution of these bands to the increasingly marked presence of Si-O-Al and of Al-O-Al bonds, respectively.

The behavior of the spectra around 570cm^{-1} and 510cm^{-1} for the series 1 glasses confirms these interpretations. The shoulder at 510cm^{-1} is only visible for the Na/Ca0.3 and Ca glasses, which can be explained by the propensity of Ca atoms (present in higher concentrations in these glasses) to regroup Al among them. Furthermore, the peak at 570cm^{-1} is present for all the glasses in the first series, which justifies its attribution to the Si-O-Al bonds.

3.1.3 Region between 825cm^{-1} and 1300cm^{-1}

Zooms on the Raman spectra for the three series of glasses in the region between 825cm^{-1} and 1300cm^{-1} are shown in Figure 3. The bands in this region of the spectra mainly come from stretching modes of the Si-O bonds.

The NBO1 glass spectrum (series 2 glass) with a low Al_2O_3 content can be used as a reference to interpret the modifications seen on the other spectra. This spectrum has two peaks at 949cm^{-1} and 1093cm^{-1}, which the literature devoted to sodium silicates has attributed to the entities Q_2 and Q_3 [44,45]. In the following the paper, the notation Q_n will refer to a four coordinated Si atom surround by n bridging oxygen, and 4-n non bridging oxygens. From the NBO1 glass to the NBO4 glass, the peak at 1093cm^{-1} shifts towards lower frequencies because of the increasing presence of Al ions in the environment of Si ions. This is in conformity with results given in the literature [14,46,47]. For the last series 2 glass (NBO5), the two peaks at 949cm^{-1} and 1093cm^{-1} overlap.

The correlation between the 1093cm^{-1} peak shift towards lower frequencies and the increase in the average number of Al atoms in the Si environment is confirmed for the series 3 glass spectra. Moreover, and again for series 3, the tendency towards an increase in the intensity of the band at about 985cm^{-1} for glasses with the highest Al_2O_3 content could be explained by the formation of Q_4-Al (i.e. Q_4 entities surrounded by a high proportion of Al), entities which are much more sensitive in Raman spectroscopy than Q_4-Si entities.

Similar peaks appear in the series 1 glasses. The peak at 1090cm^{-1} shifts towards low frequencies when CaO replaces Na_2O, because of the lower vibration frequency of a Si-O-Ca bond compared to that of Si-O-Na [48].

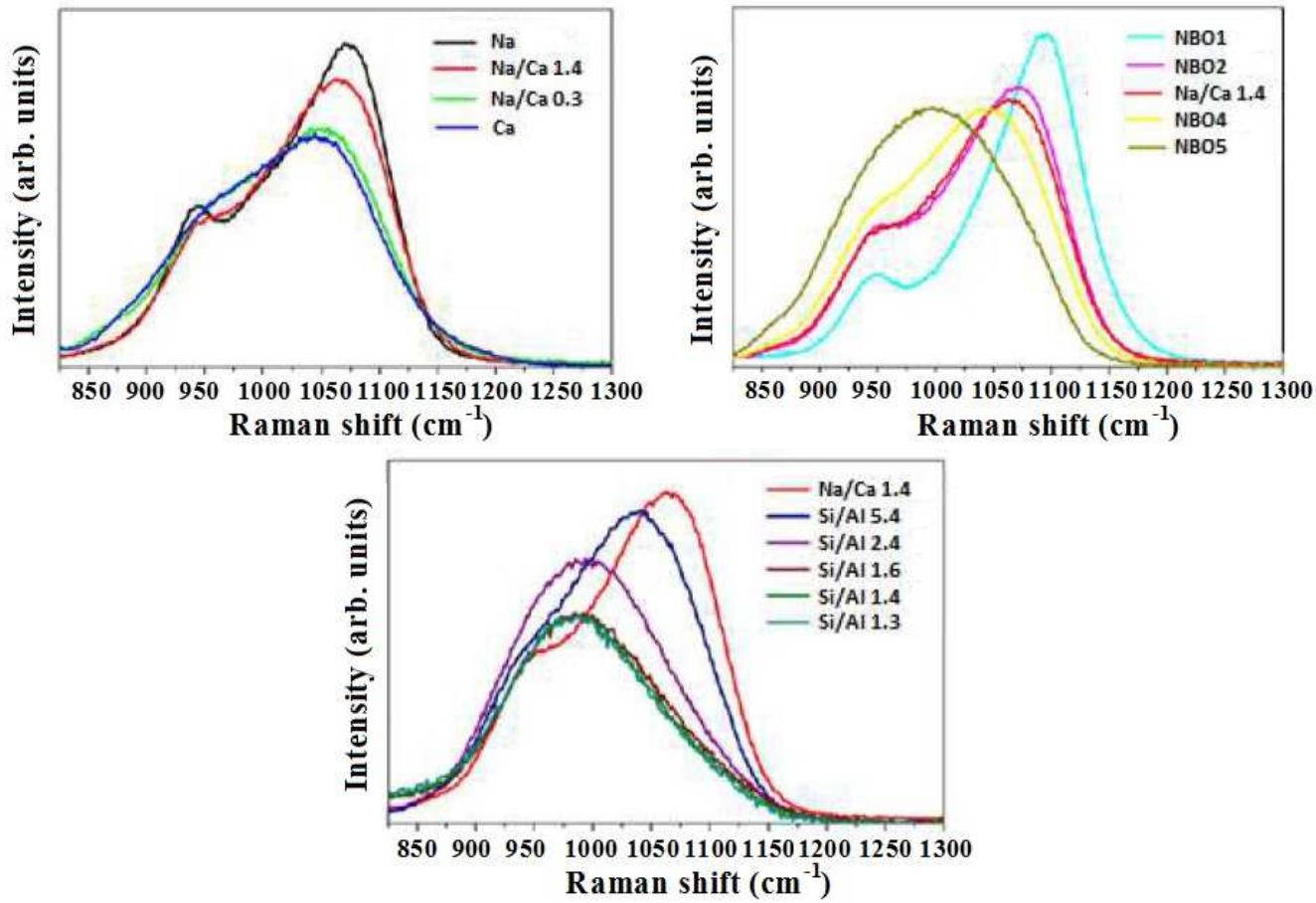

Figure 3: Raman spectra - Zoom on the region between 825cm^{-1} and 1300cm^{-1}.

3.2 NMR Spectroscopy

3.2.1 ^{27}Al NMR spectra

The ^{27}Al MAS NMR spectra (Figure 4) show that all the glasses contain tetra coordinated aluminum only, and this is confirmed by ^{27}Al MQMAS spectra (Figure 5). Strong variations between the different compositions can be clearly seen, mainly the broadening of the lines. This effect has been associated with the nature of the aluminum charge compensators (here Na^+ and Ca^{2+}) [49,50]. Indeed, as shown in 2D ^{27}Al MQMAS NMR (Figure 5), the observed variation of width of the line is mainly linked to the quadrupolar coupling constant distribution (only the spectra for the Na/Ca 1.4 and Si/Al 1.3 are shown here to present two extreme cases for the Al_2O_3 concentration). A calcium atom in the environment of tetra coordinated aluminum causes a significant increase of the quadrupolar interaction (induced by the local electric gradient), compared to a sodium atom. Thus, the observed variations can be interpreted in terms of an increasing number of calcium charge compensators around tetra coordinated aluminum. Consequently, the Ca glass which only contains Ca charge compensators showed the maximal widening. By fitting spectra with NMR parameter distribution models [9,49], variation of the NMR parameter mean values could be extracted and are plotted in Figure SI2 (see Supplementary Information).

In the first series, the Na and Na/Ca 1.4 glasses were very close, indicating the absence of calcium as charge compensator around the aluminum atoms. But for the other series 1 glasses,

for which the number of Na is close to the number of Al, a part of the Ca atoms play a charge compensator role around the Al atoms.

In the second series, it is interesting to note that in the Si/Al 1.3 glass, which did not have enough charge compensators (sodium and calcium) to compensate all the AlO_4 entities, all the Al remained tetra coordinated (the NMR spectra for the series 2 are shown in Supplementary Information).

Under these conditions, in agreement with the molecular simulations which will be presented below, the charge compensation should be ensured partially by the presence of tri coordinated oxygen.

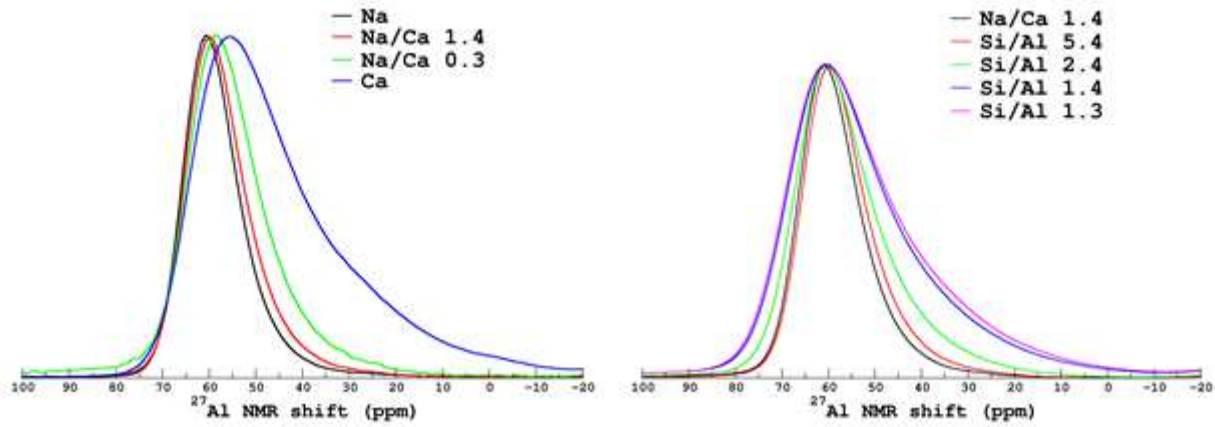

Figure 4: NMR spectra for ^{27}Al. Only glasses of series 1 and 3 are presented. The spectra for the glasses in series 2 are presented in the Supplementary Information.

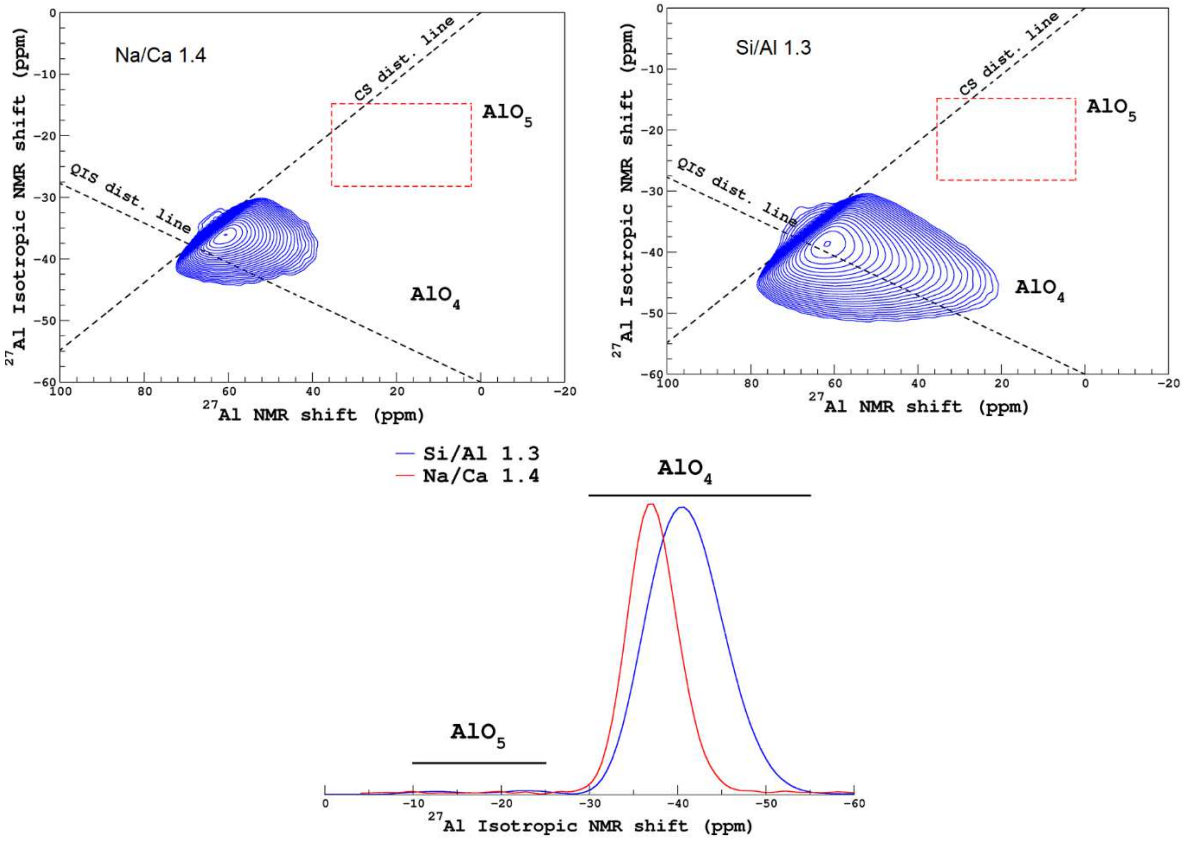

Figure 5: 2D ^{27}Al MQMAS NMR spectra for the Na/Ca 1.4 and Si/Al 1.3 glasses. Dashed lines represents the direction of spectral broadening induced by distribution of isotropic chemical shift (cs. dist. line) and quadrupolar interaction (second-order Quadrupolar Induced Shift – QIS - dist. line). These lines are helpful to determine the main contribution to the breadth of the MAS spectra. The projections on the isotropic dimension (i.e., free of second-order quadrupolar broadening) are also shown and highlight the absence of AlO_5 site.

3.2.2 ^{23}Na NMR spectra

As shown in Figure 6, ^{23}Na NMR spectra are broad, thus reflective of a widely distributed environment in term of the first-coordination (oxygen) sphere [9]. Only qualitative information can be deduced based on the relative position of the lines compared to each other. In particular, a shift towards more negative chemical shifts reflects an increase in average of the Na-O distances [40]. Positive shifts characterize sodium atom in vicinity of non-bridging oxygen atoms (shorter distances) whereas negative shifts for first-coordination dominated by bridging oxygen atoms [9,49]. In other words, ^{23}Na NMR yields positive shifts for network modifiers and negative shifts for charge compensators. Thus the average role of Na can be explained by the examination of the NMR spectra.

The spectra for the different glasses (Figure 6) show relatively few differences except for the Na/Ca 0.3 glass, which confirms that in this sample the proportion of Na as a charge compensator for Al increases. This result can be explained, as the composition contains fairly similar amounts of Al and Na.

The variation of the NMR parameter mean values have been extracted and are plotted in Figure SI4 (see Supplementary Information).

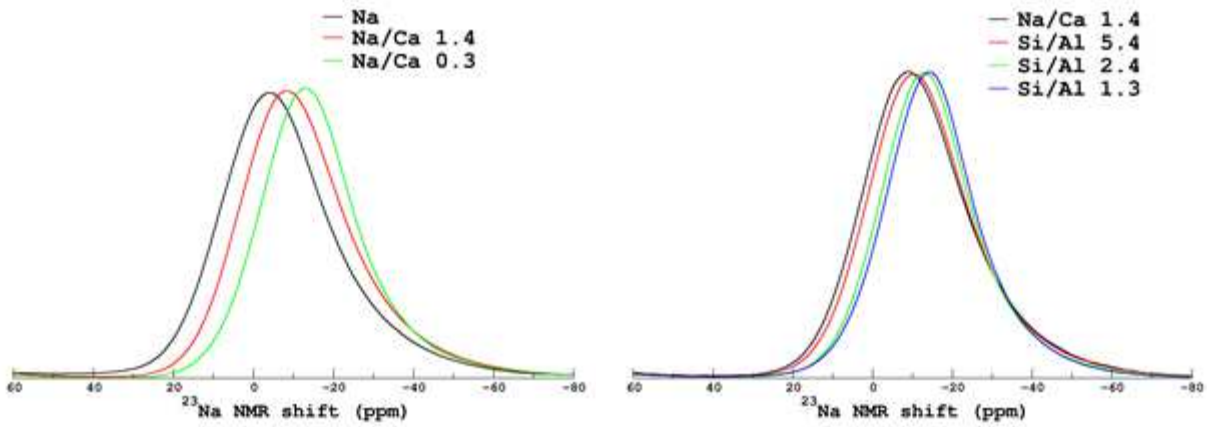

Figure 6: ^{23}Na NMR spectra for the glasses in series 1 and 3. The spectra for the glasses in series 2 are given in Supplementary Information.

3.2.3 ^{29}Si NMR spectra

The ^{29}Si MAS NMR spectra (Figure 7) show different changes in series 1 and 2 (the spectra for the series 3 are given in Supplementary Information). The observed variations can be ascribed to two major effects: the Al/Si mixing and the depolymerization of the glass network (formation of NBOs).

In series 2, the major compositional effect, the decrease of the Si/Al ratio, results in a shift to less negative NMR shifts. This is due to the increase of Al/Si bonds (one bond substitution increases the isotropic shift by approximately 3-5 ppm according to [9]).
In series 1, we observe an increase of the spectrum width and a shift toward lower NMR shifts. This shift is classically attributed to an increase of the glass polymerization. But here, the Na glass contains a large quantity of SiO_2 and a part of the Na atoms are used for the AlO_4 charge compensation so we don't expect a large NBO quantity in this glass. This result is confirmed by Molecular Dynamics calculations (paragraph 3.3.1). To explain the shift toward lower NMR shifts, the following explanation is proposed: the shift towards the left induced by the depolymerization in the Ca glass compared to the Na glass could be compensated by a shift toward the right linked to a decrease of the Si/Al mixing because of the replacement of Na_2O by CaO.
In series 3, much less variations are observed. The decrease of NBO percentage (leading to lower NMR shifts) is most probably counterbalanced by the increase due to a higher Si/Al mixing.

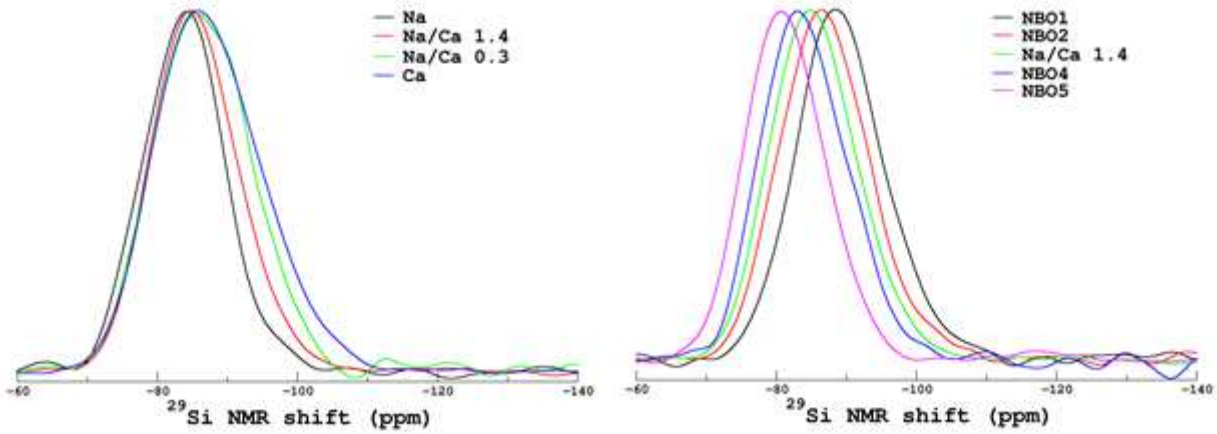

Figure 7: ^{29}Si NMR spectra for the glasses in series 1 and 2. The spectra for the glasses in series 3 are given in Supplementary Information.

3.2.4 ^{17}O NMR spectra

The Na/Ca 1.4, Si/Al 5.4 and Si/Al 2.4 glass compositions were enriched in oxygen-17 for ^{17}O MAS NMR experiments. The ^{17}O MQMAS spectra (Figure 8) show the presence of bonds between aluminum atoms (Al-O-Al) only for the glass with the highest Al content (Si/Al 2.4). For this sample, the number of Si-O-Si bonds dropped considerably while the Si-O-Al bonds increased.
This observation confirmed the Raman spectroscopy results, with the rise of the peak at 510cm^{-1} for the series 3 glasses.

For all the compositions, mixing sites were found gathering calcium and sodium atoms around non bridging oxygens. The quantification of the different contributions is given in Table 2, based on the MQMAS spectrum projection simulation in the isotropic dimension shown in supplementary materials.

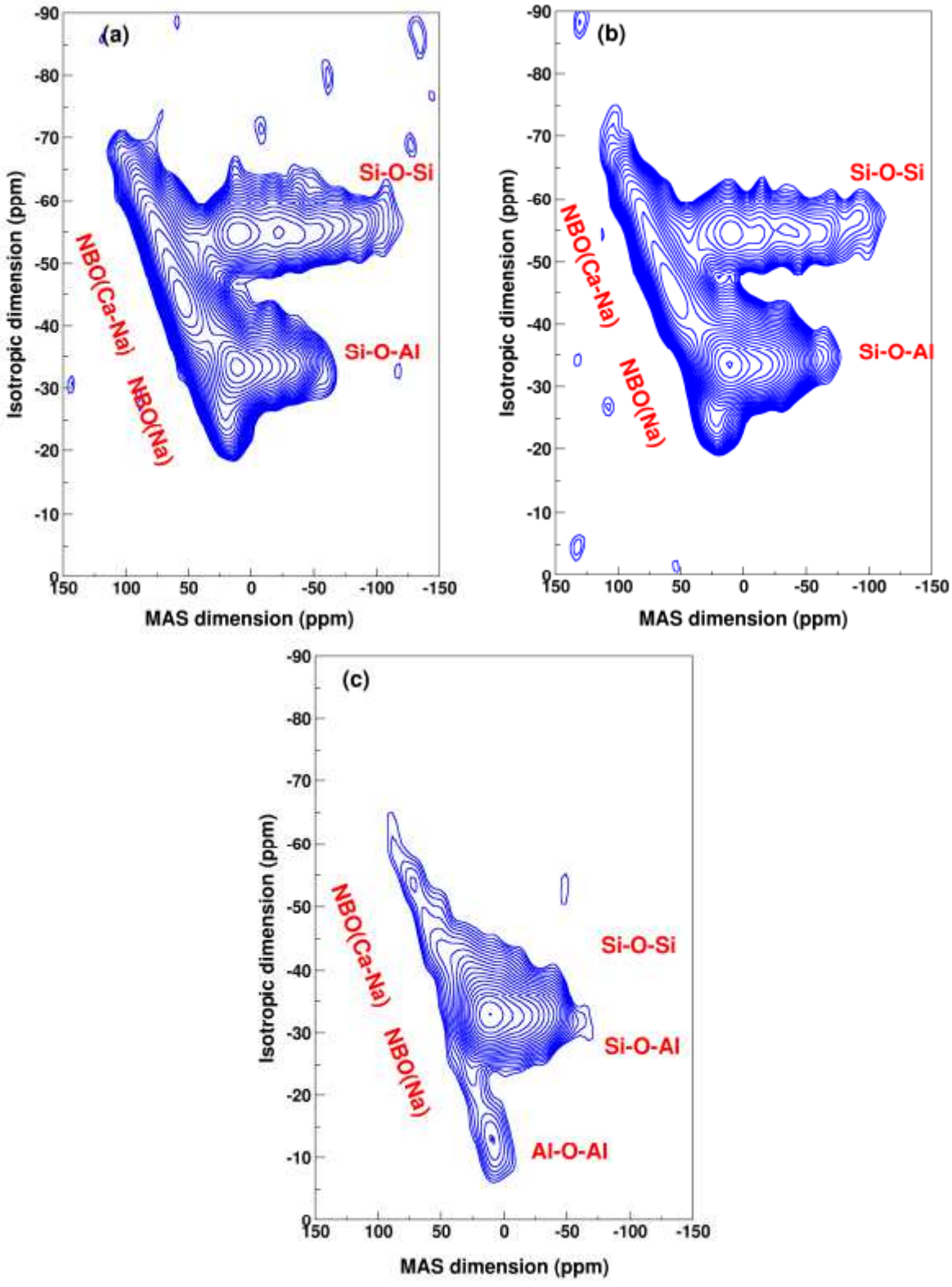

Figure 8: ^{17}O NMR spectra for the glasses (a) Na/Ca 1.4 (b) Si/Al 5.4 and (c) Si/Al 2.4.

	Si-O-Si	Si-O-Al	Al-O-Al	Si-O-Na	Si-O-Na/Ca
Na/Ca 1.4	32%	29%	-	6 %	23%
Si/Al 5.4	21%	47%	-	4%	28%
Si/Al 2.4	6%	72%	8%	3%	11%

Table 2: Percentages of Si-O-Si, Si-O-Al, Al-O-Al, Si-O-Na (NBO(Na)) , Si-O-Na/Ca (NBO (Na-Ca)) entities in the Na/Ca 1.4, Si/Al 5.4, and Si/Al 2.4 glasses. Values are extracted from ^{17}O MQMAS NMR measurements (see figure SI6-8 in Supplementary Materials).

3.3 Atomistic simulation results

The glasses simulated by molecular dynamics, whose compositions have been given in paragraph 2.3, were analyzed at the atomic scale to highlight the correlations between the short and medium range orders and the chemical compositions on the one hand, and on the other hand to compare the simulations with the experimental data previously described in order to improve their interpretations.

Before entering the details of the analysis, we have verified first that the glassy structures were globally homogenous. As an example, we have plotted on Figure 9 two snapshots of the Na/Ca 1.4 glass, a global view of the structure (Figure 9.a) and a zoom on the local organization of the chemical species (Figure9.b). The chemical species seem homogeneously distributed inside the simulation box.

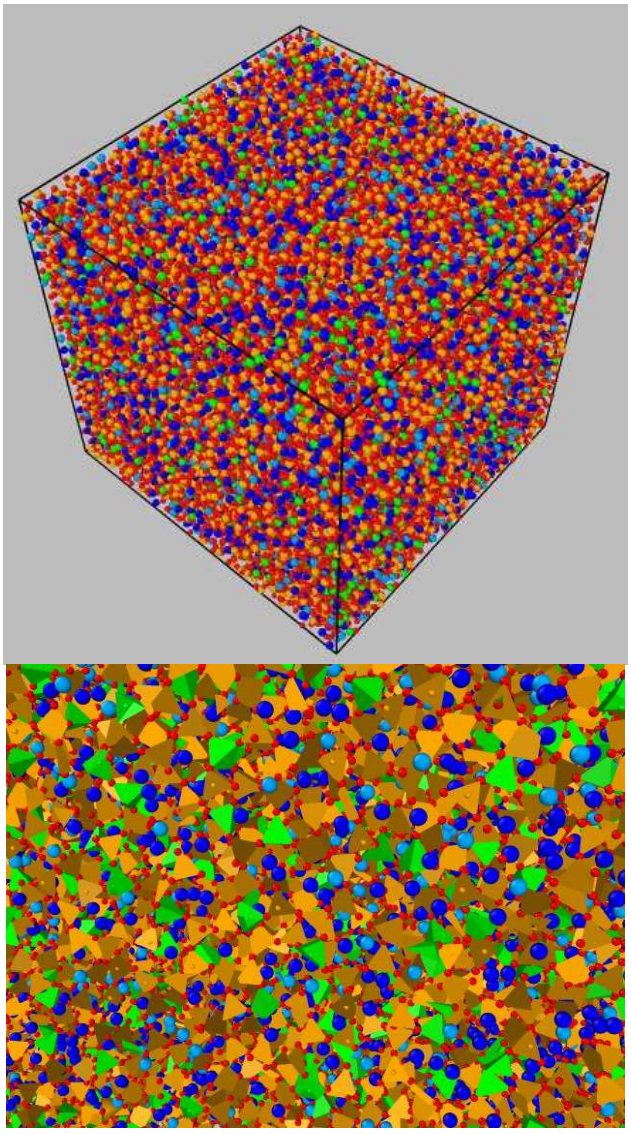

Figure 9: a. Global view of the Na/Ca 1.4 glass. Si: orange, Al: green, Na: dark blue, Ca: light blue, O: red. b. Zoom on a particular region of the glass. The coordination polyhedral around the Si (orange) and Al (green) are underlined.

3.3.1 Structural analyses at short range order

First, the connectivity of each system was measured, quantifying the percentages of 4 and 5 coordinated Si and of 3, 4 and 5 coordinated Al (Table 3).
Whatever the composition, the 5 coordinated Si concentration remains very slight, in good agreement with the experiment which concluded on a dominance of tetra coordinated Si (virtually all the Si were found to be 4 coordinated).

Most of the Al ions were found to be 4 coordinated, as had been seen experimentally, but there was nevertheless an increase in the amount of 5 coordinated Al when the Na/Ca ratio decreased. In the Na/Ca 0.3 and Ca glasses especially, the 5 coordinated Al concentrations exceeded 2%. This phenomenon, not observed for the experiments presented here, could be due to an artifact of the force fields used in molecular dynamics or to a too large quench rate. An AlO_5 environment with five bridging oxygens presents a local charge of -2. A Ca^{2+} ion enables compensation for this more easily than two Na^+ ions for steric hindrance reasons, and hence it can explain an increase in the $^{[5]}$Al content when Ca replaces Na. It can be noticed that such entities were observed in peralkaline aluminosilicate glasses previously using NMR techniques [16].

	$^{[4]}$Si	$^{[5]}$Si	$^{[3]}$Al	$^{[4]}$Al	$^{[5]}$Al
Na/Ca 1.4	99.99%	0.01%	0%	98.68%	1.32%
Na/Ca 0.3	100%	0%	0%	97.75%	2.24%
Ca	99.96%	0.04%	0.01%	94.18%	5.67%
Si/Al 5.4	100%	0%	0.01%	99.02%	0.93%
Si/Al 2.4	100%	0%	0.05%	99.28%	0.67%
Si/Al 1.3	100%	0%	0.11%	98.51%	1.34%
Na	100%	0%	0.3%	98.73%	1.27%

Table 3: Percentages of $^{[4]}$Si, $^{[5]}$Si, $^{[3]}$Al, $^{[4]}$Al, and $^{[5]}$Al in the simulated glasses.

The glass cross-links can also be studied using the number of non-bridging oxygens and the 2 or 3 coordinated oxygens (bridging oxygens). These percentages are given in Table 4.

The amount of non-bridging O increased logically with the number of free charges, i.e. with the number of modifiers (Na or Ca) not mobilized to compensate for the Al ions (the quantity of free charges (Na+2*Ca-Al) is also indicated in Table 4). This free charge quantification method is based on the chemical composition of the glass, which means it can be generalized to any composition, but it remains approximate given that the different coordination numbers around the Al atoms are not taken into consideration.

On the other hand, the 3 coordinated O content increased when the Na_2O decreased, particularly in the Si/Al 1.3 glass where the Na_2O concentration became insufficient to compensate all the Al atoms. In this glass, very few 5 coordinated Al were created (see Table 3) but the compensation for AlO_4 entities was carried out by tri-coordinated O.

	$^{[1]}$O	$^{[2]}$O	$^{[3]}$O	Free charges

Na/Ca 1.4	31.1%	68.8%	0.1%	10782
Na/Ca 0.3	33.9%	66.0%	0.2%	12168
Ca	33.2%	66.4%	0.4%	12338
Si/Al 5.4	27.1%	72.6%	0.2%	9328
Si/Al 2.4	12.3%	85.7%	2.0%	3618
Si/Al 1.3	4.1%	86.3%	9.6%	0
Na	21.8%	78.1%	0.1%	7500

Table 4: Percentages of [1]O, [2]O, and [3]O, and quantities of free charges in the simulated glasses.

A graph giving these results is shown in Figure 10. The higher the quantity of Na +2*Ca –Al, the more the non-bridging O content increases (Figure 10, top). On the contrary, the lower that quantity, the greater the tri-coordinated O content becomes (Figure 10, bottom).
Here, the simulations indirectly confirm the experimental results obtained by NMR which pointed to the absence of 5 coordinated Al in the glasses studied. From these experiments it can be deduced that in peraluminous glasses, a certain number of tetrahedral AlO_4 are locally compensated by tri-coordinated O [51,52,53,54,55].

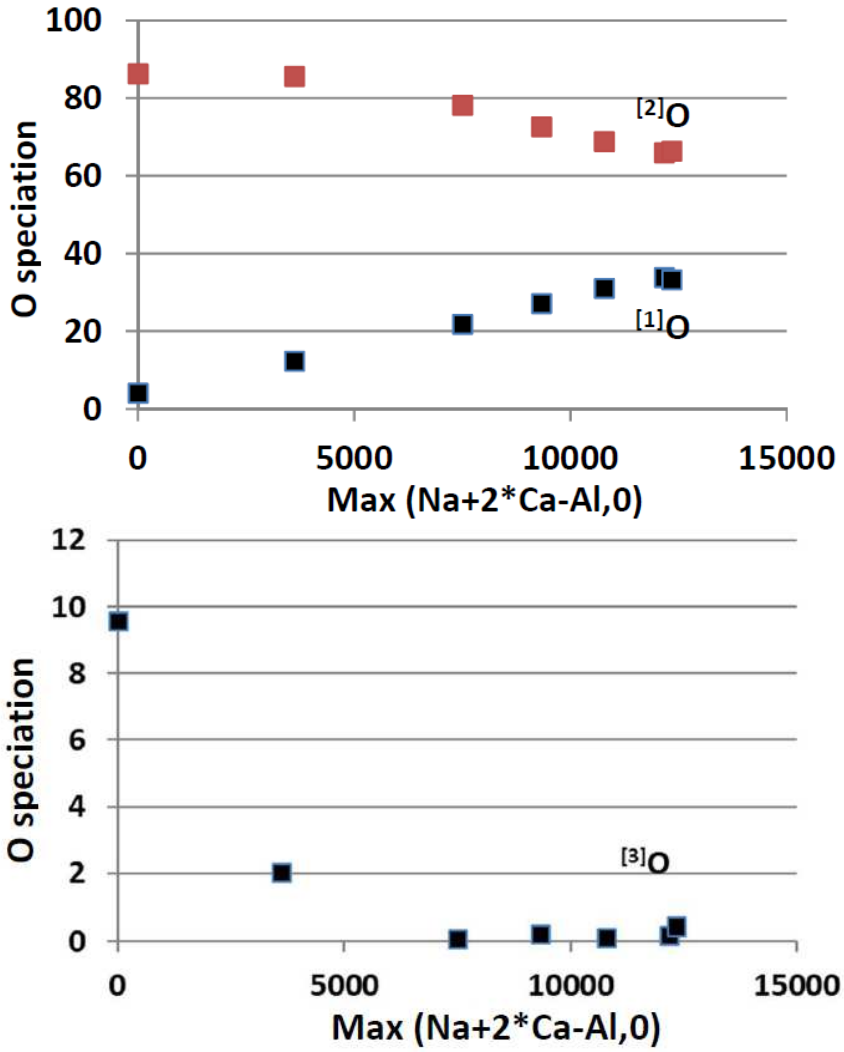

Figure 10: Percentages of [1]O, [2]O, and [3]O versus the quantity of free charges.

It is interesting to see that the non-bridging oxygens are preferentially found in the vicinity of Si rather than Al (Table 5). In fact approximately 5 times more non-bridging oxygens could be detected around the Si atoms than those around the Al. The modifiers not mobilized to compensate the AlO_4 entities are therefore positioned around the Si in priority, and form NBOs there.
This result mirrors that found experimentally, as no NBOs were found around Al [7,56].

	Si - NBO	**Al - NBO**
Na/Ca 1.4	0.86	0.15
Na/Ca 0.3	0.95	0.2
Ca	0.94	0.23
Si/Al 5.4	0.8	0.15
Si/Al 2.4	0.41	0.08
Si/Al 1.3	0.16	0.03
Na	0.58	0.07

Table 5: $^{[1]}O$ coordination around Si and Al in the simulated glasses.

Several articles in the literature, as well as the NMR analyses carried out here, conclude as to there being a preferential attraction for Na rather than Ca in the Al environments [7,8,9,10,11]. This study sought to verify this point by measuring the average coordinations in Na and Ca around the Al ions (Table 6). For this calculation, Na-Al and Ca-Al cut-off radii, respectively 4.575Å and 4.775Å, were used. These cutoff radii correspond to the positions of the minima after the first peak of the Al-Na and Al-Ca radial distribution functions.

When the ratios of the quantities of Na and of Ca present around the Al are compared with the Na/Ca global ratios for the glasses, a tendency for a preferential attraction of Na by the Al atoms emerges, but this remains only weakly present and even disappears in the glasses where the quantity of free charges lessens (Si/Al 2.4 and Si/Al 1.3 glasses). For the latter samples, the Ca becomes more attracted by the Al ions.

	$^{[Na]}$**Al**	$^{[Ca]}$**Al**	$^{[Na]}$**Al**/$^{[Ca]}$**Al**	**Na/Ca**
Na/Ca 1.4	4.06	1.30	3.12	2.89
Na/Ca 0.3	2.07	2.79	0.74	0.69
Ca	0	4.27	0	0
Si/Al 5.4	4.16	1.32	3.15	2.93
Si/Al 2.4	3.59	1.32	2.72	2.86
Si/Al 1.3	2.84	1.18	2.41	2.70
Na	5.24	0	-	-

Table 6: $^{[Na]}Al$ and $^{[Ca]}Al$ are respectively the coordinations in Na and Ca around the Al atoms. The last column indicates the Na/Ca ratio.

Table 7 gives the ratios for the percentages obtained from molecular dynamics and from NMR for the experimentally quantifiable environments.
In the Na/Ca 1.4 glass, the percentages of Si-O-Si, Si-O-Al, and Al-O-Al triplets were correctly reproduced by the MD simulations, but the overly-high proportion of Si-O-Na and the weakness of the proportion of Si-O-Ca confirm that the simulation did not correctly

reproduce the preferential attraction of Na by Al. As a result, too many Na atoms were found around the Si atoms. This situation can also be seen for the Si/Al 5.4 glass.

In the Si/Al 2.4 glass, which contained a large amount of Al_2O_3, the over-estimation of the percentage of Si-O-Si triplets and the under-estimation of the percentage of Si-O-Al triplets show that the organization between the Si and the Al was not completely reproduced by the simulation. The difficulty of compensating the charges around the AlO_4 entities in this glass seemed to lead to an artificial clustering of the Al. Again for this glass, the quantity of Si-O-Na was over-estimated, because the attraction of the Na by the Al atoms was not strong enough.

	Si-O-Si	**Si-O-Al**	**Al-O-Al**	**Si-O-Na**	**Si-O-Ca**	**Si-O-Na/Ca**
Na/Ca 1.4	0.97	1.01	(0% NMR – 1.7% MD)	1.80	0.16	1.34
Si/Al 5.4	1.06	0.85	(0% NMR – 4.4% MD)	1.95	0.19	1.23
Si/Al 2.4	1.91	0.82	3.83	0.72	0.23	0.63

Table 7: Ratios between the quantities of triplets measured by MD simulations and by ^{17}O NMR for the Na/Ca 1.4, Si/Al 5.4, and Si/Al 2.4 glasses. For the Al-O-Al triplets, the percentages are given quantitatively when no such triplets were detected by ^{17}O NMR.

To give a complete picture, the percentages of the different triplets for the glasses which were not analyzed by ^{17}O NMR spectroscopy are shown in Table 8.

	Si-O-Si	**Si-O-Al**	**Al-O-Al**	**Si-O-Na**	**Si-O-Ca**	**Si-O-Na/Ca**
Na	48.1%	28.8%	1.8%	21.4%	0%	0%
Na/Ca 0.3	39.6%	25.8%	1.8%	1.0%	11.3%	20.5%
Ca	37.5%	28.0%	2.6%	0%	31.9%	0%
Si/Al 1.3	13.4%	56.5%	26.5%	0.6%	0.5%	2.5%

Table 8: Percentages for the Si-O-Si, Si-O-Al, Al-O-Al, Si-O-Na, Si-O-Ca, and Si-O-Na/Ca triplets in the simulated glasses not analyzed for ^{17}O by NMR.

3.3.2 Medium range order analyses

A comparison between the quantities of Si-O-Si, Si-O-Al, and Al-O-Al triplets actually observed in the glasses and the estimation based on a random distribution of the ions enabled to estimate the trends for the species to gather. Figure 11 illustrates the percentage differences between the quantities measured in the simulated systems and the quantities estimated for the case of a random distribution. The method described in reference [57] was used.

Only the triplets with a 2 coordinated O were considered (triplets constructed around a 3 coordinated O were not taken into account).
A tendency for mutual exclusion among the Al was highlighted. In fact the simulated quantities of Si-O-Al and Al-O-Al were respectively higher and lower than the random estimations, which led to a trend towards mixing Si and Al in the vitreous network. This exclusion was all the more noticeable when the quantity of free charges became lower. The origin of this phenomenon has not been clearly identified, but could be linked to the increase in the O_3 content, which attracts some of the Al atoms.

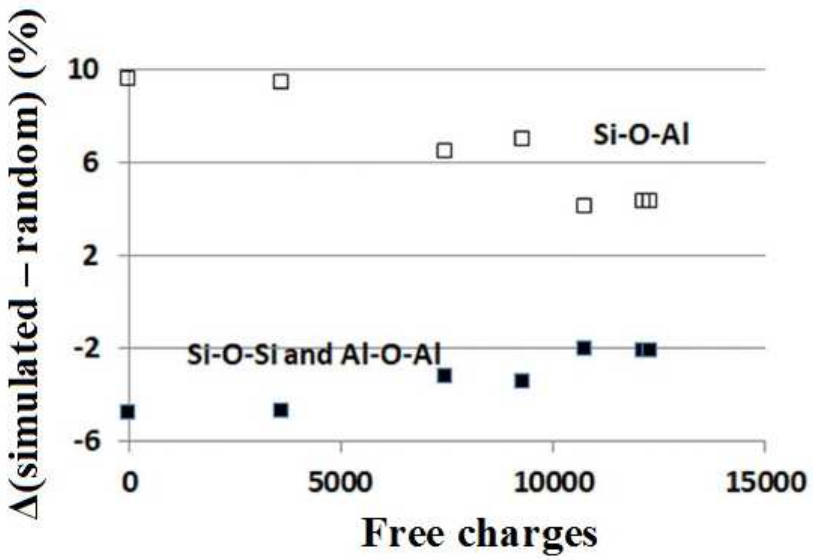

Figure 11: Difference between the percentages of Si-O-Si, Si-O-Al, and Al-O-Al measured by MD simulations and given by a random distribution model versus the quantity of free charges.

If we compare the glasses Na (7500 free charges) and Ca (12338 free charges), the Si/Al mixing is larger for the former compared to the latter. So replacing Na by Ca leads to a decrease of the Si/Al mixing, which is in agreement with the explanation proposed to explain the ^{29}Si NMR spectra measured in the glasses of series 1 (see paragraph 3.2.3).
The medium range order of the different systems can also be described by the measurement of the inter-tetrahedral angles between the SiO_4 and AlO_4 entities. Figure 12 shows the evolution of the average Si-O-Si and Si-O-Al angles versus the Si/Al ratio. The Na/Ca ratio is indicated near each point.

Two clear trends emerge. When the Na/Ca ratio remains in the interval (2.7: 2.89) but Al replaces Si, the Si-O-Si and Si-O-Al angles decrease only slightly. However when the Na/Ca ratio drops considerably in the interval (0: 2.89) but the Si/Al ratio changes very little, the Si-O-Si and Si-O-Al angles clearly decrease. This means that it is the nature of the charge compensator, Na or Ca, which has an influence on the Si-O-Si and Si-O-Al angles, rather than the respective quantities of Si and of Al. On this point the simulation resembled the Raman spectroscopy results, which showed a decrease in the Si-O-Si angle not only when affected by the replacement of Na by Ca but also because of an increase in the Al_2O_3 content to the detriment of SiO_2.

This point is coherent with what was found in the article reference [42]. The same sort of angle closing as that found in this study was observed when Ca replaced Na in silicate glasses with the composition $SiO_2 – Al_2O_3 – Na_2O – CaO$.

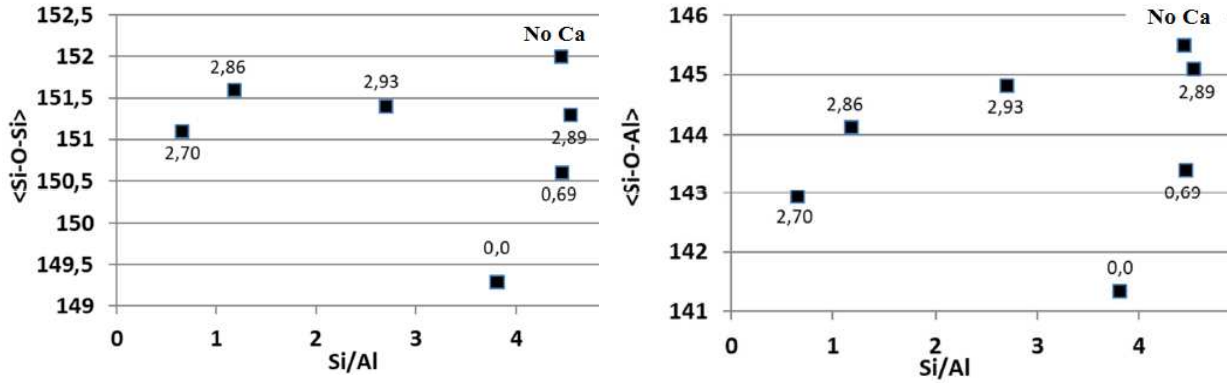

Figure 12: Si-O-Si (right) and Si-O-Al (left) average angles versus the Si/Al ratio. The Na/Ca ratio is indicated near each symbol.

4. Discussion

4.1 About Raman spectroscopy

The evolutions of the different bands in the regions between 450cm^{-1} and 825cm^{-1}, and between 825cm^{-1} and 1300cm^{-1}, point to the more important structural effects which followed the replacement of Na_2O by CaO, or the replacement of SiO_2 by Al_2O_3.
Based on molecular dynamics calculations, the decrease in the Si-O-Si angles can thus be explained both by the replacement of Na_2O by CaO and by the increase in the quantity of Al in the vicinity of the Si atoms.
In the first case, the stronger force field of Ca compared to that of Na can lead to the closing of Si-O-Si bonds. This effect is particularly significant in structures simulated by molecular dynamics. The influence of the amount of Al in the vicinity of Si on the Si-O-Si bond angles is more difficult to understand, and may be linked to questions of local energy minimization.

The effect of a greater amount of Al or Ca is an increase in the number of Al-O-Al bonds, and this is shown by a significant rise in the 510cm^{-1} band for compositions which have a high Al_2O_3 or CaO content. The Loewenstein's exclusion rule is therefore less noticeable for these compositions.

At the methodological level, the comparison of the Raman spectra from the different glass series, coupled with the ^{17}O NMR analyses, enabled more certainty in the attribution of the bands at 570cm^{-1} and 510cm^{-1} respectively to the Si-O-Al and Al-O-Al bonds. Previously, this point was a subject of controversy in the literature.

Elsewhere, higher CaO and Al_2O_3 contents have a considerable impact on the region between 825cm^{-1} and 1300cm^{-1}. The greater mass of Ca compared to Na leads to a weaker vibration frequency for the Si-O-Ca bonds than that of the Si-O-Na bonds, and hence to a shift of the 1093cm^{-1} peak towards lower frequencies. Larger amounts of Al in the vicinity of Si have the same effect.
Lastly, it should be noted that the band at about 985cm^{-1} rises significantly when the Al_2O_3 content increases. This is attributed to the formation of Q_4-Al entities, which are very sensitive in Raman spectroscopy.

4.2 About NMR spectroscopy

Unlike Raman spectroscopy, which enables access to the structural organization at the medium range order, NMR spectroscopy gives a better characterization and quantification of the local environment around the nuclei, by probing their chemical and geometric environment.

Isotopic enrichment in oxygen-17 enabled all the bridging and non bridging sites to be brought to the fore and quantified. Regions rich in non bridging oxygens within the zones enriched in sodium and calcium were highlighted. Zones where aluminum atoms gathered were observed when the number of alkali ions diminished to the benefit of the alkaline-earth ions. In these conditions, it was also seen that calcium plays the role of charge compensator in the vicinity of aluminum. The decrease of the Si/Al mixing when Na_2O is replaced by CaO is in agreement with the ^{29}Si NMR spectra measured in the series 1 and 2.

When the number of sodium atoms is high enough, this element remains the primary Al charge compensator compared to calcium in agreement with what has been observed in [11]. In all cases, aluminum retains its tetrahedral environment within NMR detection limits (< 1%). This is true even when the compensator element content is not enough to compensate all the Al atoms, in contradiction to what has been observed in [16]. It is thus natural to conclude, as confirmed by molecular modeling, that tri coordinated O form to play a compensator role for AlO_4 entities. Tri coordinated O atoms have never been directly shown by oxygen-17 NMR, as their contribution to the spectra is probably masked by other contributions.

4.3 About molecular dynamics simulations

The study carried out here by simulation targeted not just the validation of the force fields used to represent the different compositions, but also a better understanding of the different glass structures.

It is interesting to note that a certain number of experimental observations were correctly reproduced, quantitatively or sometimes simply qualitatively, but that other results conflicted with the experiments.
Concerning Al coordination, even if 5 coordinated Al were observed in simulation, especially in the glasses with a weak Na/Ca ratio, their proportions remained low. The results were therefore in good agreement with the experiments, which showed all the Al to be 4 coordinated. From this point of view, the force fields are reliable.

Also very interestingly, it was seen that the tri coordinated O content increased significantly when the quantity of charge compensators became insufficient, thus reinforcing the hypothesis that tri coordinated O can compensate AlO_4 entities.

Concerning the nature of the charge compensators around the AlO_4 entities, the simulation did not reproduce the experiment very well. Where a much stronger attraction exerted on Na compared to Ca was expected around the AlO_4 entities, only a slightly higher attraction was observed here. This underlines the difficulty in using Buckingham-type force fields to correctly represent the relative interactions between the different cations.

All the Si atoms were 4 coordinated, in agreement with the experimental data.
The smaller Si-O-Si angle due to a decreased Na/Ca ratio or an increased Al_2O_3 content was correctly reproduced, with the simulation predicting a stronger effect for the Na/Ca ratio. The

two origins for the decreasing Si-O-Si angle identified by Raman were therefore confirmed. It should be noted that this effect was also observed for the Si-O-Al angles.

The molecular simulation confirmed that non bridging oxygens are preferentially located around tetrahedral SiO_4 rather than tetrahedral AlO_4. Elsewhere, mixed sites with the combined presences of Na and Ca around NBOs were detected, in conformity with the NMR results and with previous observations [11].

The percentages of Si-O-Si, Si-O-Al, and Al-O-Al bridging sites were quantified by ^{17}O NMR in three glass compositions. The results were compared to the simulation. When the Al_2O_3 content was low, the comparison was satisfactory. For the glass with a 20.7% Al_2O_3 content (Si/Al 2.4 glass), the difference rose, revealing the difficulty for these force fields to accurately reproduce the organization of the alumino-silicate network of very aluminum-rich glasses.
Despite the difficulties to reproduce the precise Si-O-Si, Si-O-Al and Al-O-Al quantities, the simulation is able to reproduce the decrease of the Si/Al mixing when Na_2O is replaced by CaO, as suggested by the ^{29}Si NMR results.

Finally, it appears that globally the force fields used reproduce the glass structural characteristics quite well, in spite of the existence of certain differences concerning the relative interactions between Na and Ca or between Al and Si. More precise potentials, like polarizable potentials or those constructed digitally on the basis of ab initio calculations (Machine Learning) [58,59] would probably enable these inaccuracies to be corrected.

5. Conclusions

To prepare for a study into the effects of ballistic irradiation on SiO_2-Al_2O_3-Na_2O-CaO glasses under consideration for the storage of radioactive waste, a preliminary study was carried out in order to characterize their structures. Several series of glasses were defined to cover a wide range of compositions among the peralkaline and peraluminous glasses. A number of complementary techniques were implemented: Raman and NMR spectroscopy, and classical molecular dynamics.
The compositions selected were chosen to determine the effect of the progressive replacement of Na_2O by CaO, or of SiO_2 by Al_2O_3, as well as the effect of an increasing Al_2O_3 content.

The following results were obtained:
- Absence of 5 or 6 coordinated Al, whatever the composition. Compensation for the negative charge of AlO_4 entities could occur via the formation of tri coordinated O.
- Decrease in the Si-O-Si and Si-O-Al angles when Ca replaced Na or when the Al/(Si+Al) ratio increased.
- Presence of Al-O-Al bonds observed, as well as an increase in their content when the Al or Ca concentrations increased.
- Confirmation of the preferential compensation in AlO_4 entities by Na rather than by Ca.
- Presence of non bridging oxygens with a mixed environment containing both Na and Ca.

Concerning the experimental methodology, the comparison of the Raman and NMR spectra acquired from the different series of glasses enabled the Raman band at 570cm^{-1} to be attributed to Si-O-Al bonds, and that at 510cm^{-1} to Al-O-Al bonds. As for the Raman band at 985cm^{-1}, it can be attributed to the presence of Q_4-Al entities.

Concerning the molecular modeling study, comparisons between experimental findings and simulated structures were used to check that a large number of experimental behaviors can be correctly reproduced by the classical potential recently developed by Deng et al. It was found that a certain lack of precision remains as to the relative interactions between Na and Ca, and between Si and Al, making the reproduction of certain phenomena such as the preferential attraction of Na by AlO_4 or the increase in the number of Al-O-Al bonds in glasses with a high Al_2O_3 content more challenging.

Acknowledgements

The authors wish to sincerely thank ORANO, France, EDF, France and the CEA, France, for their financial support during this study.

REFERENCES

[1] A. Le Gac, B. Boizot, C. Jegou, S. Peuget, Nucl. Instrum. Methods Phys. B, 407 (2017) 203-209.
[2] P. Chevreux, A. Laplace, E. Deloule, L. Tissandier, N. Massoni, J. Non-Cryst. Solids, 457 (2017) 13-24.
[3] G. Agnello, R. Youngman, L. Lamberson, N. Smith, W. LaCourse, A.N. Cormack, J. Non-Cryst. Solids, 519 (2019) 85-95.
[4] L. Cormier, D.R. Neuville, Chem. Geol., 213 (2004) 103-113.
[5] D.R. Neuville, L. Cormier, A.-M. Flank, V. Briois, D. Massiot, Chem. Geol., 213 (2004) 153-163.
[6] D.M. Zirl, S.H. Garofalini, J. Am. Ceram. Soc., 73 (1990) 2848-2856.
[7] J.R. Allwardt, S.K. Lee, J.F. Stebbins, AM. Mineral, 88 (2003) 949-954.
[8] A. Pedone, Int.J. Quantum Chem., 116 (2016) 1520-1531.
[9] E. Gambuzzi, A. Pedone, M.C. Menziani, F. Angeli, D. Caurant, T. Charpentier, Geochim. Cosmochim. Acta, 125 (2014) 170-185.
[10] A. Pedone, E. Gambuzzi, G. Malavasi, M.C. Menziani, Theor. Chem. Acc., 131 (2012) 1147.
[11] S.K. Lee, S. Sung, Chem. Geol., 256 (2008) 326.
[12] L.M. Thompson, J.F. Stebbins, J. Non-Cryst. Solids, 358 (2012) 1783-1789.
[13] L.M. Thompson, J.F. Stebbins, Am. Mineral., 96 (2011) 841-853.
[14] D.R. Neuville, L. Cormier, D. Massiot, Geochim. Cosmochim. Acta, 68 (2004) 5071-5079.
[15] D.R. Neuville, L. Cormier, D. Massiot, Chem. Geol., 229 (2006) 173-185.
[16] S.K. Lee, G.D. Cody, B.O. Mysen, Am. Mineral. 90 (2005) 1393.
[17] W. Loewenstein, Am. Mineral., 39 (1954) 92-96.
[18] L. Cormier, D. Ghaleb, D.R. Neuville, J.-M. Delaye, G. Calas, J. Non-Cryst. Solids, 332 (2003) 255-270.
[19] S.K. Lee, J.F. Stebbins, Am. Mineral., 84 (1999) 937-945.
[20] J.F. Stebbins, Nature, 330 (1987) 465-467.
[21] C. Le Losq, D.R. Neuville, W. Chen, P. Florian, D. Massiot, Z. Zhou, G.N. Greaves, Sci. Rep., 7 (2017) 16490.
[22] G.N. Greaves, S. Sen, Adv. Phys., 56 (2007) 1-166.
[23] G.N. Greaves, K.L. Ngai, Phys. Rev. B, 52 (1995) 6358-6380.
[24] F. Lodesani, M.C. Menziani, H. Hijiya, Y. Takato, S. Urata, A. Pedone, Sci. Rep., 10 (2020) 2906.
[25] A. Jan, J.-M. Delaye, S. Gin, S. Kerisit, J. Non-Cryst. Solids, 505 (2019) 188-201.
[26] A. Pedone, G. Malavasi, M.C. Menziani, A.N. Cormack, U. Segre, J. Phys. Chem. B, 110 (2006) 11780 – 11795.
[27] L. Deng, J. Du, J. Am. Ceram. Soc., 102 (2018) 2482-2505.
[28] S. Sundararaman, L. Huang, S. Ispas, W. Kob, J. Chem. Phys., 150 (2019) 154505.
[29] B. Guillot, N. Sator, Geochim. Cosmochim. Acta, 71 (2007) 1249-1265.
[30] M.T. Ha, S.H. Garofalini, J. Am. Ceram. Soc., 100 (2017) 563-573.
[31] Y. Xiang, J.C. Du, M.M. Smedskjaer, J.C. Mauro, J. Chem. Phys., 139 (2013) 044507.
[32] A. Tilocca, N.H. de Leeuw, A.N. Cormack, Phys. Rev. B, 73 (2006) 104209.
[33] D.A. Long, Raman Spectroscopy, Mc-Graw Hill International Book Company, New York, 1977.
[34] J. P. Amoureux, C. Fernandez, S. Steuernagel, J. Magn. Reson. A, 123 (1996) 116.
[35] D. Massiot, B. Touzo, D. Trumeau, J. P. Coutures, J. Virlet, P. Florian, P.J. Grandinetti, Solid State Nucl. Magn. Reson., 6 (1996) 73.
[36] F.H. Larsen F. H., I. Farnan (2002), Chem. Phys. Lett., 357 (2002) 403.
[37] W. Smith, I. Todorov, Mol. Simul., 32 (2007) 935-943.
[38] L. Deng, J. Du, J. Non-Cryst. Solids, 453 (2016) 177-194.

[39] L.-H. Kieu, J.-M. Delaye, L. Cormier, C. Stolz, J. Non-Cryst. Solids, 357 (2011) 3313–3321.
[40] C. Le Losq, D.R. Neuville, P. Florian, G.S. Henderson, D. Massiot, Geochim. Cosmochim. Acta 126 (2014) 495-517.
[41] E.I. Kamitsos, J.A. Kapoutsis, H. Jain, C.H. Hsieh, J. Non-Cryst. Solids, 171 (1994) 31-45.
[42] F. Angeli, J.-M. Delaye, T. Charpentier, J.-C. Petit, D. Ghaleb, P. Faucon, Chem. Phys. Lett., 320 (2000) 681-687.
[43] X. Xue, J. Stebbins, Phys. Chem. Minerals, 20 (1993) 297.
[44] S.A. Brawer, W.B. White, J. Non-Cryst. Solids, 23 (1977) 261-278.
[45] T. Furukawa, J. Chem. Phys., 75 (1981) 3226-3237.
[46] P. McMillan, B. Piriou, J. Non-Cryst. Solids, J. Non-Cryst. Solids, 53 (1982) 279-298.
[47] B.O. Mysen, Structure and properties of silicate melts, Elsevier Science and Technology Books, Amsterdam, 1988.
[48] D.R. Neuville, Chem. Geol., 229 (2006) 28-41.
[49] F. Angeli, M. Gaillard, P. Jollivet, T. Charpentier, Chem. Phys. Lett., 440 (2007) 324-328.
[50] M. Licheron, V. Montouillout, F. Millot, D.R. Neuville, J. Non-Cryst. Solids, 357 (2011) 2796-2801.
[51] J.D. Kubicki, M.J. Toplis, Am. Mineral., 87 (2002) 668-678.
[52] A. Atila, E. Ghardi, A. Hasnaoui, S. Ouaskit, J. Non-Cryst. Solids, 525 (2019) 119470.
[53] M. Benoit, M. Profeta, F. Mauri, C.J. Pickard, M.E. Tuckerman, J. Phys. Chem. B, 109 (2005) 6052-6060.
[54] J.F. Stebbins, J.V. Oglesby, S. Kroeker, Am. Mineral., 86 (2001) 1307-1311.
[55] N. Jakse, M. Bouhadja, J. Kozaily, J.W.E. Drewitt, L. Hennet, D.R. Neuville, H.E. Fischer, V. Cristiglio, A. Pasturel, Appl. Phys. Lett., 101 (2012) 201903.
[56] E.I. Morin, J.F. Stebbins, J. Non-Cryst. Solids, 471 (2017) 179-186.
[57] J.-M. Delaye, L. Cormier, D. Ghaleb, G. Calas, J. Non-Cryst. Solids, 293 (2001) 290.
[58] F. Pacaud, M. Salanne, T. Charpentier, L. Cormier, J.-M. Delaye, J. Non-Cryst. Solids, 499 (2018) 371-379.
[59] Z. Chaker, M. Salanne, J.-M. Delaye, T. Charpentier, Phys. Chem. Chem. Phys., 21 (2019) 21709-21725.